Multiscale asymptotic-based modeling of local material inhomogeneities

Eduard Marenić, Delphine Brancherie, Marc Bonnet

8th International Congress of Croatian Society of Mechanics
29 September – 2 October 2015
Opatija, Croatia

Multiscale asymptotic-based modeling of local material inhomogeneities

Eduard MARENIĆ*, Delphine BRANCHERIE*, Marc BONNET+

**Laboratoire Roberval, Université de Compiegne, Centre de Recherches de Royallieu*
60203 Compiegne, France
E-mails: {eduard.marenic,delphine.brancherie}@utc.fr

+*ENSTA, POems, Unité de Mathématiques Appliquées, 828 boulevard des Marechaux,*
91120 Palaiseau, France
E-mails: mbonnet@ensta.fr

Abstract. This research is a first step towards designing a numerical strategy capable of assessing the nocivity of a small defect in terms of its size and position in the structure with low computational cost, using only a mesh of the defect-free reference structure. The proposed strategy aims at taking into account the modification induced by the presence of a small inhomogeneity through displacement field correction using an asymptotic analysis. Such an approach would allow to assess the criticality of defects by introducing trial micro-defects with varying positions, sizes and mechanical properties.

1 Introduction

The role played by defects in the initiation and development of rupture is crucial and has to be taken into account in order to realistically describe the behavior till complete failure. The difficulties in that context revolve around (i) the fact that the defect length scale is much smaller than the structure length scale, and (ii) the random nature of their position and size. Even in a purely deterministic approach, taking those defects into consideration by standard models imposes to resort to geometrical discretisations at the defect scale, leading to very costly computations and hindering parametric studies in terms of defect location and characteristics.

Our current goal is to design an efficient two-scale numerical strategy which can accurately predict the perturbation in terms of displacement concentration caused by an inhomogeneity in elastic (background) material given by elasticity tensor ($\boldsymbol{\mathcal{C}}$). To make it computationally efficient, the analysis uses only a mesh for the defect-free structure, i.e. the mesh size does not depend on the (small) defect scale. The latter is instead taken into account by means of a multiscale asymptotic expansion (see e.g. [4, 5]), in which the concept of *elastic moment tensor* (EMT) [3, 1] plays an important role.

2 Problem definition

The main feature of the proposed approach is as briefly stated in the introduction to accurately predict the perturbation caused by an inhomogeneity in elastic (background)

material, without explicitly modeling it. That is, we consider an elastic body occupying a smooth bounded domain $\Omega \subset \mathbb{R}^3$ characterized by elasticity tensor $\boldsymbol{\mathcal{C}}$, as depicted in Figure 1 a), and we seek the solution of the background problem, given below. Having this solution in hand, we proceed with the asymptotic expansion of the displacement perturbation. Adding these two elements together should correspond to what we call the transmission (perturbed) problem, without really solving it. The transmission problem for a small trial inhomogeneity involves a small elastic ($\boldsymbol{\mathcal{C}}^\star$) inhomogeneity located at $\mathbf{z} \in \Omega$, of characteristic linear size a, occupying the domain $B_a := \mathbf{z} + a\mathcal{B}$, where $\mathcal{B} \subset \mathbb{R}^3$ is a smooth fixed domain centered at the origin and defines the inhomogeneity shape, see Figure 1 b). The elastic properties of the whole solid are defined as

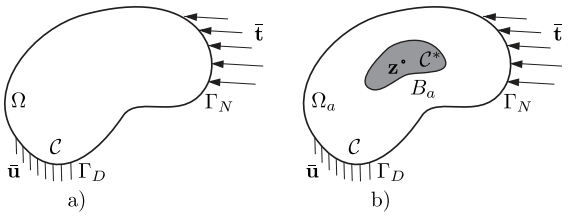

Figure 1: Model scheme showing the geometric setting, that is, unperturbed a) and perturbed b) domains, Ω and Ω_a, respectively. The inhomogeneity B_a located at $\mathbf{z}$ is the shaded subdomain in (b).

$$\boldsymbol{\mathcal{C}}_a := \boldsymbol{\mathcal{C}}\chi_{\Omega\setminus B_a} + \boldsymbol{\mathcal{C}}^\star\chi_{B_a}, \tag{1}$$

where χ_D is the characteristic function of a domain D. For the later reference we also introduce the material contrast, or elastic tensor perturbation, as $\Delta\boldsymbol{\mathcal{C}} = \boldsymbol{\mathcal{C}}^\star - \boldsymbol{\mathcal{C}}$.

Background solution. The background solution in terms of displacement field $\mathbf{u}$ arising in the reference solid Ω due to prescribed excitation $(\mathbf{f}, \bar{\mathbf{t}}, \bar{\mathbf{u}})$, is defined by the problem

$$\operatorname{div}(\boldsymbol{\mathcal{C}} : \boldsymbol{\varepsilon}[\mathbf{u}]) + \mathbf{f} = \mathbf{0} \text{ in } \Omega, \quad \mathbf{t}[\mathbf{u}] = \bar{\mathbf{t}} \text{ on } \Gamma_N, \quad \mathbf{u} = \bar{\mathbf{u}} \text{ on } \Gamma_D, \tag{2}$$

where Γ_N and Γ_D typically denote Neumann and Dirichlet parts of boundary, while $\boldsymbol{\varepsilon}[\mathbf{w}]$ and $\mathbf{t}[\mathbf{w}]$ are linearized strain tensor and traction vector associated with a given displacement $\mathbf{w}$, which are defined as

$$(a) \quad \boldsymbol{\varepsilon}[\mathbf{u}] = \nabla_{\text{sym}}\mathbf{u}, \quad (b) \quad \mathbf{t}[\mathbf{u}] = (\boldsymbol{\mathcal{C}} : \boldsymbol{\varepsilon}[\mathbf{u}]) \cdot \mathbf{n}, \tag{3}$$

with $\mathbf{n}$ being the unit outward normal to Γ_N.

Transmission solution The displacement field $\mathbf{u}_a$ arising in the solid containing the small inhomogeneity B_a due to the same prescribed excitation $(\mathbf{f}, \bar{\mathbf{t}}, \bar{\mathbf{u}})$, solves the transmission problem with elastic properties distributed as in (1)

$$\text{(a) } \operatorname{div}(\boldsymbol{\mathcal{C}}_a : \boldsymbol{\varepsilon}[\mathbf{u}_a]) + \mathbf{f} = \mathbf{0} \text{ in } \Omega, \quad \text{(b) } \mathbf{t}[\mathbf{u}_a] = \bar{\mathbf{t}} \text{ on } \Gamma_N, \quad \text{(c) } \mathbf{u} = \bar{\mathbf{u}}_a \text{ on } \Gamma_D, \tag{4}$$

where the perfect-bonding transmission conditions are implicitly enforced via (4a) written in the distributional sense and the usual smoothness assumption $\mathbf{u}_a \in H^1(\Omega)$.

Multiscale approach by asymptotic expansion. Let us first define the displacement perturbation

$$\mathbf{v}_a := \mathbf{u}_a - \mathbf{u}, \tag{5}$$

as the difference of the total and unperturbed displacement corresponding to problems (4) and (2), respectively. Two distinct asymptotic expansions of $\mathbf{v}_a$ arise, namely a *near-field* and a *far-field* expansion. This distinction naturally involves two scales: the "scale a" corresponding to characteristic length a of the inhomogeneity, and the "scale 1" on the size of structure. This multiscale character of the asymptotic expansions is schematically depicted in the Figure 2. Furthermore, this description requests two variables [5, 4]:

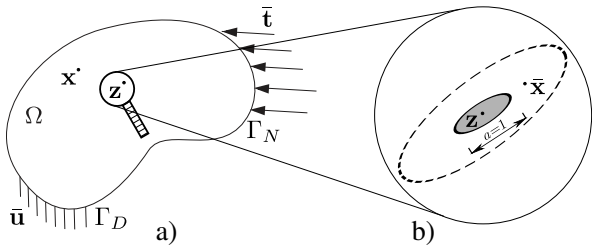

Figure 2: Scheme showing the *far-field* a) and *near-field* b) expansions. Far-field is represented with coordinates at the structure scale, while the near-field represents zoom on the ihomogenity represented by coordinates at the structure scale.

- '$\mathbf{x}$' representing coordinates at the structure scale (see Fig. 2 a)), and
- '$\bar{\mathbf{x}} := (\mathbf{x} - \mathbf{z})/a$' representing coordinates at the defect scale (see Fig. 2 b)).

The near-field expansion is given by

$$\mathbf{v}_a(\mathbf{x}) = a\mathbf{v}_{\mathcal{B}}(\bar{\mathbf{x}}) + o(a), \tag{6}$$

where $\mathbf{v}_{\mathcal{B}}$ is the solution in terms of displacement perturbation of the auxiliary problem of a perfectly bonded inhomogeneity $\mathcal{B}$ embedded in an infinite elastic medium $\Omega = \mathbb{R}^3$ and subjected to the constant remote stress $\boldsymbol{\mathcal{C}} : \nabla\mathbf{u}(\mathbf{z})$. Such solutions $\mathbf{v}_{\mathcal{B}}$ are known analytically for simple inhomogeneity shapes (see [8]) in which case they correspond to the famous Eshelby inclusion problem [6]. Expansion (6) is valid for finite $\bar{\mathbf{x}}$, i.e. within a neighbourhood of B_a whose linear size is $O(a)$. More precisely, the solution (6) represents a zoom on the ihomogeneity and thus it exists on the "scale a" (see Fig. 2 a)).

The far-field expansion, on the other hand, is given by

$$\mathbf{v}_a(\mathbf{x}) = -\nabla_1\boldsymbol{G}(\mathbf{z},\mathbf{x}) : \boldsymbol{\mathcal{A}}(\mathcal{B},\boldsymbol{\mathcal{C}},\Delta\boldsymbol{\mathcal{C}}) : \nabla\mathbf{u}(\mathbf{z})a^3 + o(a^3), \qquad \mathbf{x} \neq \mathbf{z}, \tag{7}$$

and is valid at a finite (independent on a) distance from the inhomogeneity, that is, on the scale of the structure. In this work, as a first step, we address the computation of

the far-field approximation (7) for given inclusion location $\mathbf{z}$ (thus purely deterministic approach) and varying evaluation point $\mathbf{x}$. The key "ingredients" of the far-field expansion (7) in terms of displacement perturbation are: the gradient of the background solution on the inhomogeneity site $\nabla \mathbf{u}(\mathbf{z})$, Green's tensor for the domain Ω denoted as $\boldsymbol{G}(\mathbf{z}, \mathbf{x})$ (i.e. it's gradient with respect to the first argument $\nabla_1 \boldsymbol{G}(\mathbf{z}, \mathbf{x})$), and the elastic moment tensor (EMT) $\boldsymbol{\mathcal{A}}(\mathcal{B}, \boldsymbol{\mathcal{C}}, \Delta\boldsymbol{\mathcal{C}})$. We proceed with the brief introduction, definition and properties of these quantities.

Elastostatic Green's tensor. The elastostatic Green's tensor $\boldsymbol{G}(\boldsymbol{\xi}, \mathbf{x})$ is defined as a solution of

$$\operatorname{div}(\boldsymbol{\mathcal{C}} : \boldsymbol{\varepsilon}[\boldsymbol{G}(\cdot, \mathbf{x})]) + \delta(\cdot - \mathbf{x})\mathbf{I} = \mathbf{0} \text{ in } \Omega, \quad \mathbf{t}[\boldsymbol{G}(\cdot, \mathbf{x})] = \mathbf{0} \text{ on } \Gamma_N, \quad \boldsymbol{G}(\cdot, \mathbf{x}) = \mathbf{0} \text{ on } \Gamma_D. \tag{8}$$

Defined this way Green's tensor gathers the three linearly independent elastostatic displacement fields $\boldsymbol{G}^k(\cdot, \mathbf{x})$ resulting from unit point forces $\delta(\cdot - \mathbf{x})\mathbf{e}_k$ applied at $\mathbf{x} \in \Omega$ along direction k. We further introduce a decomposition of $\boldsymbol{G}$ as

$$\boldsymbol{G}(\cdot, \mathbf{x}) = \boldsymbol{G}_\infty(\cdot - \mathbf{x}) + \boldsymbol{G}_c(\cdot, \mathbf{x}), \tag{9}$$

where $\boldsymbol{G}_\infty$ is the singular, infinite-space Green's tensor, such that

$$\operatorname{div}(\boldsymbol{\mathcal{C}} : \boldsymbol{\varepsilon}[\boldsymbol{G}_\infty]) + \delta\mathbf{I} = \mathbf{0} \text{ in } \mathbb{R}^3, \quad |\boldsymbol{G}_\infty(\xi - \mathbf{x})| \to 0 \text{ as } |\xi - \mathbf{x}| \to \infty, \tag{10}$$

and the complementary Green's tensor $\boldsymbol{G}_c$ is bounded at $\xi = \mathbf{x}$ and represents a correction of $\boldsymbol{G}_\infty$ due to the finite size of Ω. More precisely, by a superposition argument, $\boldsymbol{G}_c$ solves the elastostatic boundary-value problem (BVP) with regular boundary data and zero body force density:

$$\operatorname{div}(\boldsymbol{\mathcal{C}} : \varepsilon[\nabla \boldsymbol{G}_c]) = \mathbf{0}, \quad \nabla \boldsymbol{G}_c = -\nabla \boldsymbol{G}_\infty \text{ on } \Gamma_D, \quad \mathbf{t}[\nabla \boldsymbol{G}_c] = -\mathbf{t}[\nabla \boldsymbol{G}_\infty] \text{ on } \Gamma_N, \tag{11}$$

where the boundary data is related to the trace of $\nabla \boldsymbol{G}_\infty$ on $\partial\Omega$, treated columnwise as displacement fields, and the traction vectors associated with those displacements. Note that problem (11) is posed directly i terms of the gradient of complementary Green's tensor, mainly to avoid the loss of accuracy caused by numerical derivative (see [7] for details). Note also that problem (11) in fact involves 9 loading cases for 3D conditions (and 4 for 2D conditions).

Elastic moment tensor (EMT). The EMT [1] is the key mathematical concept in the asymptotic expansion of $\mathbf{v}_a$. It carries important microstructural information, namely the material contrast $\Delta\boldsymbol{\mathcal{C}}$, the inhomogeneity shape $\mathcal{B}$ and its orientation (see e.g. Definition 2.3. in [3] for details and properties of the EMT). We focus in this work on the EMT $\boldsymbol{\mathcal{A}}$ associated with an *ellipsoidal* inhomogeneity $(\mathcal{B}, \boldsymbol{\mathcal{C}} + \Delta\boldsymbol{\mathcal{C}})$ embedded in a medium with elasticity tensor $\boldsymbol{\mathcal{C}}$, which is given by [3]

$$\boldsymbol{\mathcal{A}} = |\mathcal{B}|\boldsymbol{\mathcal{C}} : (\boldsymbol{\mathcal{C}} + \Delta\boldsymbol{\mathcal{C}} : \boldsymbol{\mathcal{S}})^{-1} : \Delta\boldsymbol{\mathcal{C}}, \tag{12}$$

where $\boldsymbol{\mathcal{S}} = \boldsymbol{\mathcal{S}}(\mathcal{B}, \boldsymbol{\mathcal{C}})$ denotes the (fourth-order) Eshelby tensor of the inclusion $\mathcal{B}$ [8]. We will be dealing in this paper with the special case of plane strain, corresponding to an ellipsoidal inclusion $\mathcal{B}$ infinitely elongated in the x_3 direction, assuming $\boldsymbol{\mathcal{C}}$ and $\boldsymbol{\mathcal{C}}^\star$ to be both isotropic. In this case, the nonzero components of the Eshelby tensor $\boldsymbol{\mathcal{S}}$ are given explicitly as

$$\begin{aligned} S_{1111} &= A(1-m)(3+\gamma+m), \qquad & S_{1122} &= A(1-m)(1-\gamma-m), \\ S_{2222} &= A(1-m)(3+\gamma-m), \qquad & S_{2211} &= A(1+m)(1-\gamma+m), \\ S_{1212} &= A(1+m^2+\gamma), \end{aligned} \tag{13}$$

where $A = 1/[8(1-\nu)]$, $\gamma = 2(1-2\nu)$, and $m = (a_1 - a_2)/(a_1 + a_2)$, with a_1 and a_2 denoting the semi-axes of the ellipse $\mathcal{B}$ in principal directions x_1 and x_2, respectively (while $a_3 \to \infty$).

3 Numerical example

The capabilities of the proposed strategy are illustrated on the academic example involving the biaxial load of the square-shaped membrane as shown on Fig. 3. This pre-

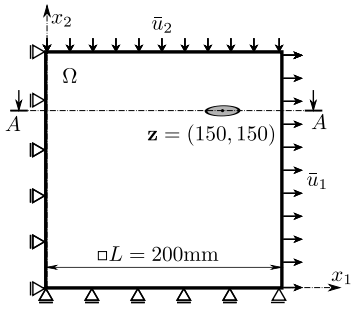

Figure 3: Scheme of the geometry and boundary conditions of the biaxially loaded square membrane.

liminary example, concerns a plane strain case involving a single, local, elliptic inhomogeneity, and will be used to further clarify the procedure and demonstrate the performance of the proposed strategy. The example of finite element meshes of unperturbed (M_0) and reference (M_r) models are shown on the Figure 4.

Proposed approach considers first the FE computation of the background solution $\mathbf{u}$ defined by problem (2) using a coarse mesh, M_0 shown on Fig. 4a). In this computation the inhomogeneity is not taken into account. Following steps of the proposed strategy aim to correct $\mathbf{u}$ by adding far field correction (7). Thus, for a given inhomogeneity position ($\mathbf{z} \in \Omega$) we first extract the gradient of the background displacement $\nabla\mathbf{u}(\mathbf{z})$. Next, we turn to the computation of the Green's tensor considering a decomposition (9). The infinite part is in our case of isotropic background material a simple derivative of the textbook fundamental (Kelvin) solution, given in (4.57) in [2]. The same infinite part serves as a

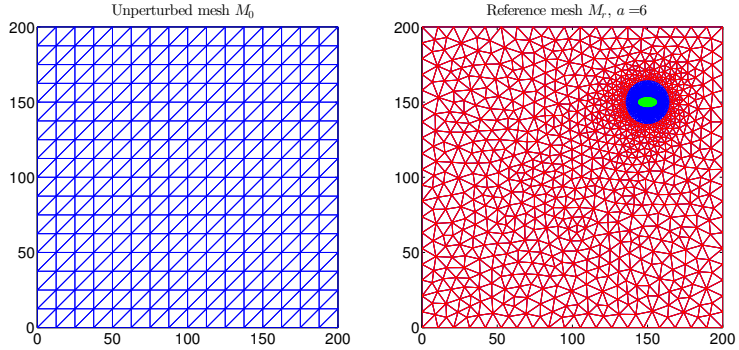

Figure 4: Finite element mesh of unperturbed i.e. background a) and reference models b). The unperturbed mesh consists of 289, and reference of 2464 nodes.

BC for complementary part (11), thus a special attention needs to be given to the preparation and correct imposition of these BC's (see [7]). With the properly defined BC's, the computation of the complementary part (11) is performed numerically using finite element method. This step also considers a finite element computations without any (fine) meshing at the defect scale.

Finally, for the given shape and material properties $(\mathcal{B}, \boldsymbol{\mathcal{C}}^\star)$ of the inhomogeneity we compute the EMT $\boldsymbol{\mathcal{A}}(\mathcal{B}, \boldsymbol{\mathcal{C}}, \Delta\boldsymbol{\mathcal{C}})$ using (12). Note, that for the case of isotropic background and inhomogeneity this can be solved analticaly, that is without any additional computation.

Having these results in hand, all the ingredients required for evaluation of the far-field asymptotic approximation (7) of $\mathbf{v}_a$ are available, and this solution may be post-processed for evaluating the defect criticality. Obtained results are to be compared with reference solution performed on a really fine mesh M_r given in th Fig. 4b). Reference model explicitly models the inhomogeneity, and is considered as a solution of the transmission problem (4), denoted as $\mathbf{u}_a^{num}$ (or in terms of perturbation $\mathbf{v}_a^{num}$). Note that the proposed approach avoids any computation on the fine mesh, both $\mathbf{u}$ and $\nabla\boldsymbol{G}_c$ are computed on M_0 (other steps pertain merely on the evaluation of analytical expressions). Approach based on asymptotic expansion takes, thus, a fraction (about 11%) of CPU time needed for the reference solution. We will discuss further the accuracy and convergence of the proposed approach.

Accuracy. The comparison of our asymptotic approximation $\mathbf{v}_a$ and referential numerical solution $\mathbf{v}_a^{num}$ are given first along the characteristic crossection $A - A$, shown on the scheme in Fig. 3. The inhomogeneity is in this case taken simply as circular hole, and a perfect agreement is achieved, solution obtained by asymptotic expansion coincides with the referential solution on the evaluation points $\mathbf{x}_0$ (see Figure 5 (left)). Moreover, to verify further proposed approach we proceed with computing the far-field asymptotic approximation (7) also on fine mesh M_r, i.e., for each node $\mathbf{x}_r$ of the fine mesh. As mentioned

above, background solution and complementary part of the Green's tensor are computed on the coarse mesh M_0, and we can using the FE interpolation $\boldsymbol{\varphi}$ write

$$\mathbf{v}_a(\mathbf{x}_r) = -(\nabla G_\infty(\mathbf{x} = \mathbf{x}_r) + \boldsymbol{\varphi} \nabla G_c(\mathbf{x}_0)) : \boldsymbol{\mathcal{A}} : \nabla \mathbf{u}(\mathbf{z}) a^3, \qquad \mathbf{x}_r, \mathbf{x}_0 \neq \mathbf{z}. \tag{14}$$

Let the difference of the two fields on the fine mesh M_r be given as $\mathbf{v}_e = \mathbf{v}_a^{num} - \mathbf{v}_a$. Then, the comparison can be given as contour plot in Figure 5 (right). This plot shows a good agreement over the whole domain, with the negligible error appearing only in the close vicinity of the inhomogeneity.

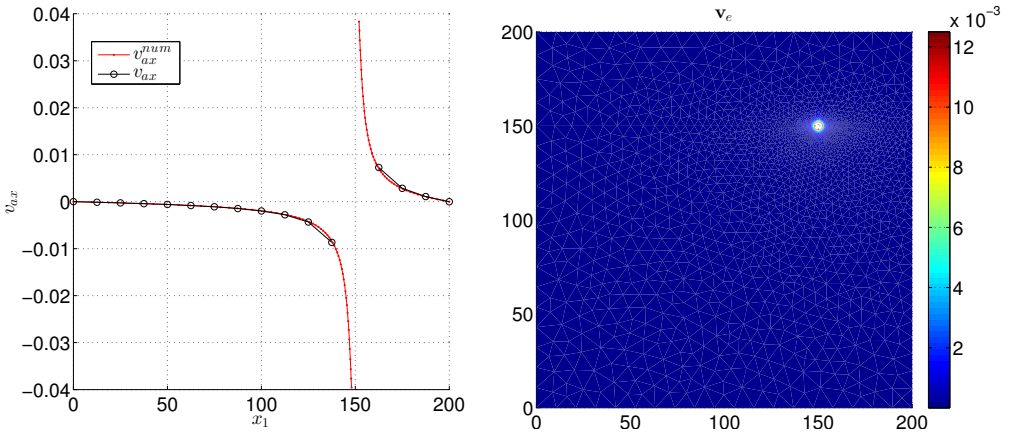

Figure 5: The comparison of the asymptotic approximation $\mathbf{v}_a$ and reference solution $\mathbf{v}_a^{num}$, along crossection $A - A$ (left), and in terms of contour plot of perturbation error $\mathbf{v}_e$ (right). Both are given for a membrane with a circular hole on site $\mathbf{z}$ of radius $a = 2$ mm.

Convergence. The proposed approach shows a good performance both in terms of efficiency and accuracy. We proceed here with the convergence test again by comparison of the asymptotic approximation with the reference results, but here for the varying characteristic inhomogeneity size a. The reference results for various inhomoeneity types and varying sizes a were made using really fine FE model (like on Figure 4 (right)). While each of this computations inherits the mentioned problems of the severe mesh refinement and cost, we can note in this convergence study the *key advantage* of the proposed approach based on asymptotic expansion (7) and the multiplicative decomposition therein. The decomposition makes possible that the information about the (virtual) inhomogeneity is stored in EMT independently from Green's tensor and background solution given by $\nabla \mathbf{u}$. Thus, asymptotic approximation for varying inhomogeneity sizes, types (here shown only ellipsoidal) and material contrasts, boils down to simple recomputing of the EMT following (12). The computation of EMT for ellipsoidal inhomogeneity (12) mainly hinges on the evaluation of Eshelby tensor $\boldsymbol{\mathcal{S}}$, which for the isotropic background material covered within this work concerns merely analytic expressions. While already for a single run our approach was taking just a fraction of the computational cost of the fine FE model, for multiple runs there is practically no added cost! This way we can achieve a significant

speed-up in predicting the perturbation caused by varying inhomogeneity sizes, types and material contrasts, which is of great practical interest.

For the convergence analysis we define discrepancy of reference and asymptotic solutions as

$$R(a) = \frac{||\mathbf{v} - \mathbf{v}_a^{num}||}{a^2} = \frac{||\mathbf{v}_e||}{a^2} = o(1). \tag{15}$$

In order to find a $O(a^2)$ remainder in (15), which is the outer asymptotic behavior of the solution, we evaluated $R(a)$ using a L_2 norm

$$||\mathbf{v}_e||_{L_2} = \int_{\Omega \backslash D} \mathbf{v}_e \mathbf{v}_e^{\mathrm{T}} d\Omega, \tag{16}$$

over a domain $\Omega \backslash D$, where D is a fixed neighbourhood around inhomogeneity. In this case we have choosen a disk with a radius R_d centered at the inhomogeneity (as shown for one a size in Figure 4b), with R_d kept fixed as a varies. The plot of $R(a)$ versus the normalized characteristic size of the inhomohenity a/L is depicted in Figure 6 for the varying inhomogeneities. We show the results for soft ($E^\star/E = 0.5$), hard ($E^\star/E = 1.5$), and nearly rigid ($E^\star/E = 10$) inhomogeneities of circular ($a_1/a_2 = 1$) and ellipsoidal ($a_1/a_2 = 2$) shape. A desired convergence trend ($O(a^2)$) is clearly visible for all considered cases.

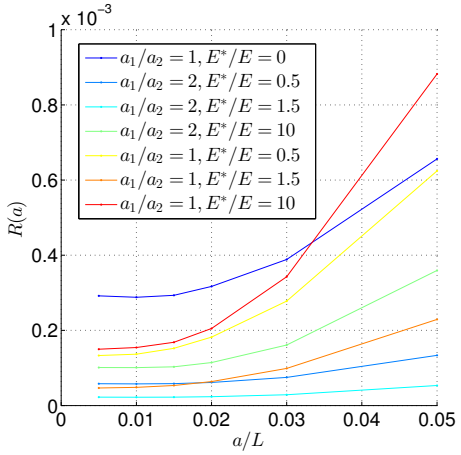

Figure 6: The plot of discrepancy versus the normalized inhomogeneity size. The soft and hard inclusions with elliptic and circular shape are considered.

4 Conclusion and perspectives

A numerical strategy for predicting the perturbation caused by an inhomogeneity in an elastic solid is outlined. We focus on the evaluation of the far field displacement correction. Thanks to the use of an asymptotic expansion, we achieve the major advantage which pertains to the fact that the defect scale is not meshed. The computations involved are straightforward and include the computation of background solution, followed by the

Green's and elastic moment tensors. A very good performance in terms of accuracy and convergence is presented on the academic example.

The next steps of this work include (i) matching the near and far-field asymptotic expansions to obtain uniform expansions, and (ii) applying the developed strategy to assessing the criticality of defects by considering virtual micro-defects and varying their positions, sizes and mechanical properties.

References

[1] H. Ammari and H. Kang. *Polarization and Moment Tensors: with Applications to Inverse Problems and Effective Medium Theory*. Springer-Verlag, New York, Applied Mathematical Sciences Series Vol. 162s, 2007.

[2] M. Bonnet. *Boundary Integral Equation Methods for Solids and Fluids*. John Wiley and Sons, Inc, 1999.

[3] M. Bonnet and G. Delgado. The topological derivative in anisotropic elasticity. *Q J Mechanics Appl Math*, 66(4):557–586, 2013.

[4] D. Brancherie, M. Dambrine, G. Vial, and P. Villon. Effect of surface defects on structure failure: a two-scale approach. *European Journal of Computational Mechanics*, 17(5-7):613624, 2008.

[5] M. Dambrine and G. Vial. A multiscale correction method for local singular perturbations of the boundary. *ESAIM: Mathematical Modelling and Numerical Analysis*, 41(1):111–127, 2007.

[6] J. D. Eshelby. The determination of the elastic field of an ellipsoidal inclusion and related problems. *Proc. R. Soc. Lond. A*, 241:376–396, 1957.

[7] E. Marenić, D. Brancherie, and M. Bonnet. Asymptotic analysis for the multiscale modeling of defects in mechanical structures. Submitted to International Journal of Solids and Structures, 2015.

[8] T. Mura. *Micromechanics of Defects in Solids*. Martinus Nijhoff Publishers, 1987.